CHAPTER 6

Robot-Assisted Cold and Warm Incremental Sheet Forming of Aluminum Alloy 6061: A Comparative Study

6.1 Introduction

Temperature plays an important role in ISF. Forming at elevated temperature positively affects ISF in terms of improved formability, decreased force, and better accuracy of the formed product. On the basis of forming temperature, forming can be classified in three categories.

(a) Cold forming: forming at room temperature

(b) Hot forming: forming at temperature greater than recrystallization temperature.

(c) Warm forming: forming at temperature greater than recrystallization temperature.

In this Chapter, robot-assisted cold incremental sheet forming (RACISF) and robot-assisted warm incremental sheet forming (RAWISF) have been performed on AA 6061. The simulation study of both the processes have been first carried out on ABAQUS and forming forces have been compared. Once the simulation got carried out successfully, experiments were conducted for RACISF and RAWISF with a six-axis industrial robotic arm. For performing RAWISF, heating of sheet has been done by using hot air gun. The path planning has been performed by online programming using a teach pendant. Several shapes have been formed, and the forming force, maximum wall angle, tensile properties, microhardness, and surface finish are compared. It is found that process capability of RAWISF is better than that of RACISF.

6.2 Simulation study

Before experimentation, both CISF and WISF have been simulated using ABAQUS V6.13 software. The simulation analysis has been carried out on a conical shape formed on the ABAQUS V6.13 platform. Three-part instances have been created: (a) the forming tool, (b) a plate made of aluminum alloy, and (c) a flange to hold the plate. The properties of the aluminum alloy 6061 are given in Table 6.1.

Table 6.1: Details of parameters used in simulation

Properties Used in Simulation	Values
Density	2.7 g/cc
Young's modulus	70 GPa
Poisson's ratio	0.33
Yield strength	249 MPa
Coefficient of friction between tool and blank	0.2
Hardening model used	Isotropic
Mesh size	6.96 mm
Mesh type	Square

The data of stress–plastic strain has been obtained from uniaxial tensile test. As tensile properties vary with test temperature, the tensile test has been carried out on a machine, equipped with a furnace for heating the sample. The setup for testing is shown in Figure 6.1.

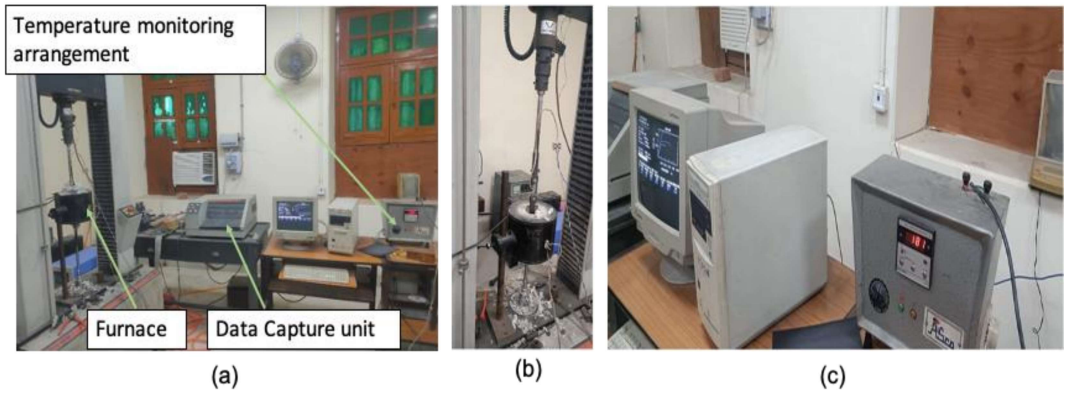

Figure 6.1: (a) Setup for tensile testing with heating furnace, (b) Sample with furnace, and (c) Temperature monitoring system.

The tensile stress–strain curves of the samples in undeformed condition are shown in Figure 6.2 (a).

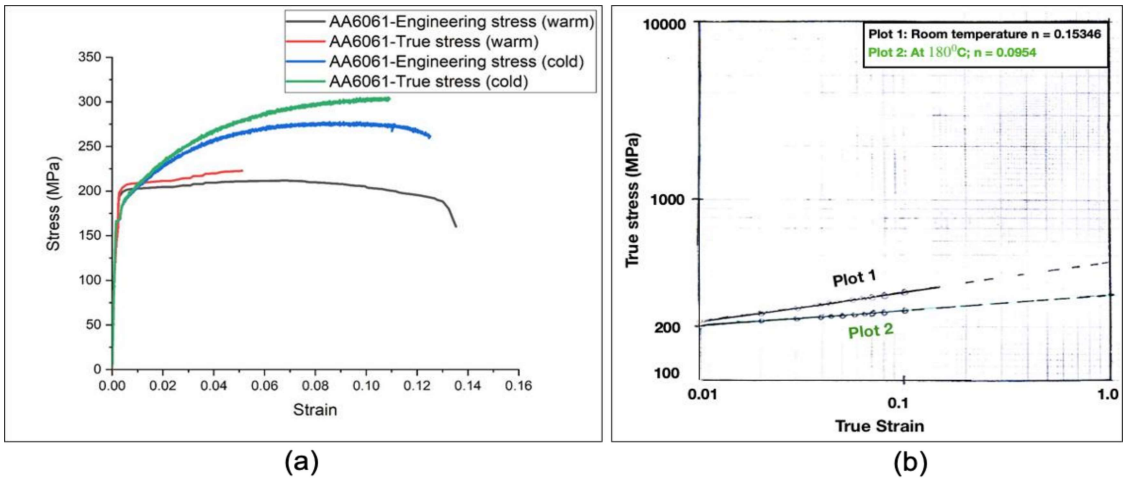

Figure 6.2: (a) Engineering and true-stress–strain curves for undeformed AA6061 sheet at room temperature and 180 °C, and (b) log–log plot of true stress–true plastic strain up to true strain = 1.0.

Once the tensile properties had been obtained from the tensile test, the respective data of true stress–true plastic strain have been used for simulation of CISF and WISF until the maximum load at which necking occurred. The log–log plot of true stress and true strain has been extended up to a strain of 1.0, as shown in Figure 6.2 (b). The value of the work hardening exponent, post-necking, has been obtained by finding the slope of this segment of the plot.

For analysis purpose, isotropic hardening and penalty contact between the tool and sheet have been taken. The friction coefficient has been taken as 0.2, obtained from the wear test. Square meshing has been done on the plate with an average mesh size of 6.96 mm. For analysis, the square blank of thickness 1.5 mm is taken. Rigid tool was made of 10 mm diameter. The geometries used with the ABAQUS simulation, including dimensions of the part, are shown in Figure 6.3.

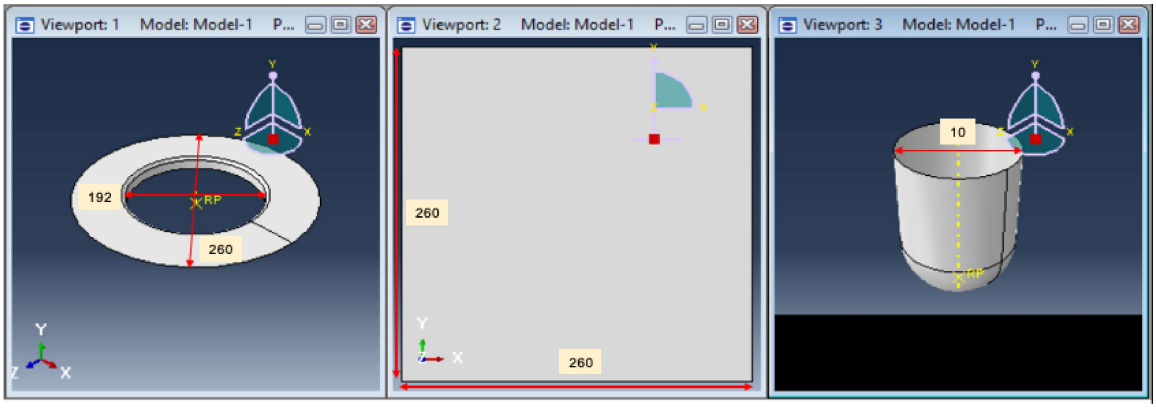

Figure 6.3: Parts used in ABAQUS with dimensions in mm: (a) Tool holder, (b) Sheet, and (c) Forming tool.

The temperature in the case of WISF forming has been maintained at 180 °C. The tool path for both CISF and WISF has been generated on MATLAB, and the position coordinates obtained have been fed in ABAQUS to obtain the conical shape. The simulation has been

run, and dynamic analysis is carried out for stresses, strains, and tool forces arising during the tool motion, the results of which are shown in Figure 6.4.

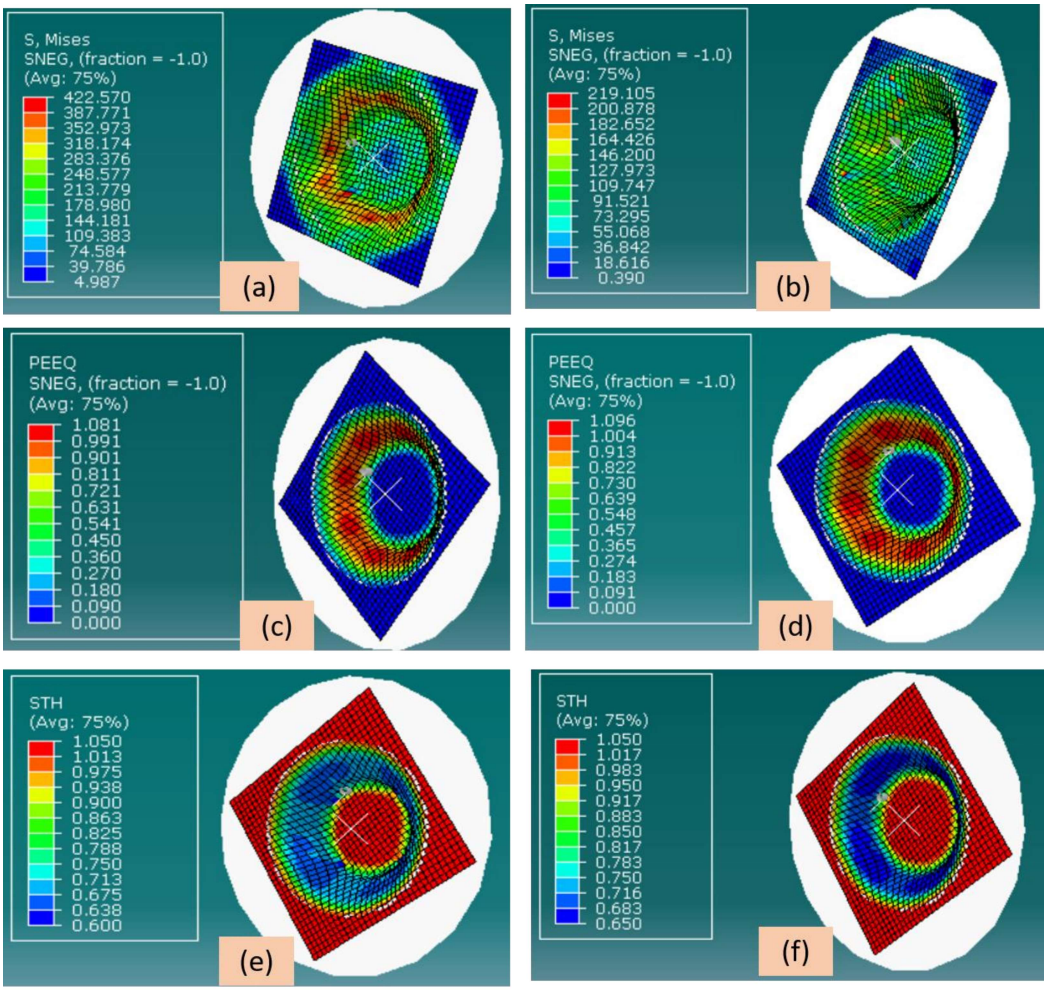

Figure 6.4. Simulation results of analysis on ABAQUS: (a) stress distribution in fabricated cone by CISF, (b) stress distribution in fabricated cone with CISF, (c) strain distribution in fabricated cone by CISF, (d) strain distribution in fabricated cone in WISF, (e) thickness variation along the wall of the formed cone in CISF, and (f) thickness variation along the wall of the formed cone in WISF.

It can be seen from Figure 6.4(a) and 6.4(b) that the Von-Mises stress is most significant in direct contact between the undeformed sheet and the tool for both CISF and WISF. The

stress distribution in both cases follows the same trend; however, the Von-Mises stress arising in CISF is more than that arising in WISF, which can lower forming forces in the case of WISF. Figure 6.4(c) and 6.4(d) illustrate that the most prominent strain occurred in middle of the cone. In WISF, the strain obtained was slightly more than that in CISF. Further, it can be revealed from Figure 6.4(e) and 6.4(f) that the central section of the cone has the minimum thickness, indicating that this region underwent the maximum amount of thinning, affirming the distribution shown in Figure 6.4(a) – (d).

6.3 Materials and methodology

After successful FEA analysis of the process on ABAQUS, the obtained results have been validated by experiments conducted on sheets of aluminum alloy 6061, with a thickness of 1.05 mm, as this is the most widely used material in the sheet metal industry. Tensile parameters have been obtained from the uniaxial tensile test. The composition of the aluminum alloy 6061 determined by an optical emission spectrometer is presented in Table 6.2.

Table 6.2: Chemical composition of the Al alloy 6061.

Elements	Al	Ti	Si	Mg	Fe	Mn	Zn	Cr	Cu
Composition (wt %)	97.76	0.05	0.71	0.89	0.21	0.11	0.09	0.06	0.0.12

Tensile tests have been conducted before forming to evaluate tensile properties of the undeformed sheet. ASTM/E8 standard has been followed in preparing the samples for the tensile test. Following ASTM/E643/15 standards, specimens for the Erichsen ductility test were prepared.

Tensile properties of the sheet of the alloy 6061, before forming into various shapes, are listed in Table 6.3.

Table 6.3: Tensile Properties of the Al alloy 6061 in heat-treated condition, before deformation.

Mechanical Properties	Values
0.2% offset yield strength (MPa)	249.30
UTS (MPa)	274.56
Elongation (%)	14.50

6.4 Experimental study

The experimental setup of robot-assisted incremental sheet forming (RAISF) has been established from scratch, at the IIT (BHU), in the production engineering lab. The main parts of the setup are (a) a six-axis industrial robot provided by M/s Yaskawa having a payload capacity of 180 kN with a controller and teach pendant; (b) the clamping arrangement; (c) a tool dynamometer for measurement of forming forces; (e) the addition of forming tool(s) for performing RAWISF heating arrangement, which consists of a heating gun and temperature-measuring infrared thermometer. The sheet was heated to a warm condition using the heating gun, and the infrared thermometer was used to measure the temperature. The schematic diagram of the experimental setup is shown in Figure 6.5. For tool path planning, the teach pendant based method has been adopted as explained in Chapter 2. The forming has been carried out with the parameters optimized by straight groove test as reported in Chapter 2. For RAWISF, a temperature of 180 °C was conveniently achieved by a hot air gun, without any sophisticated arrangement to be

mounted on a conventional RAISF setup. Once the setup was established, experiments were conducted to form various shapes.

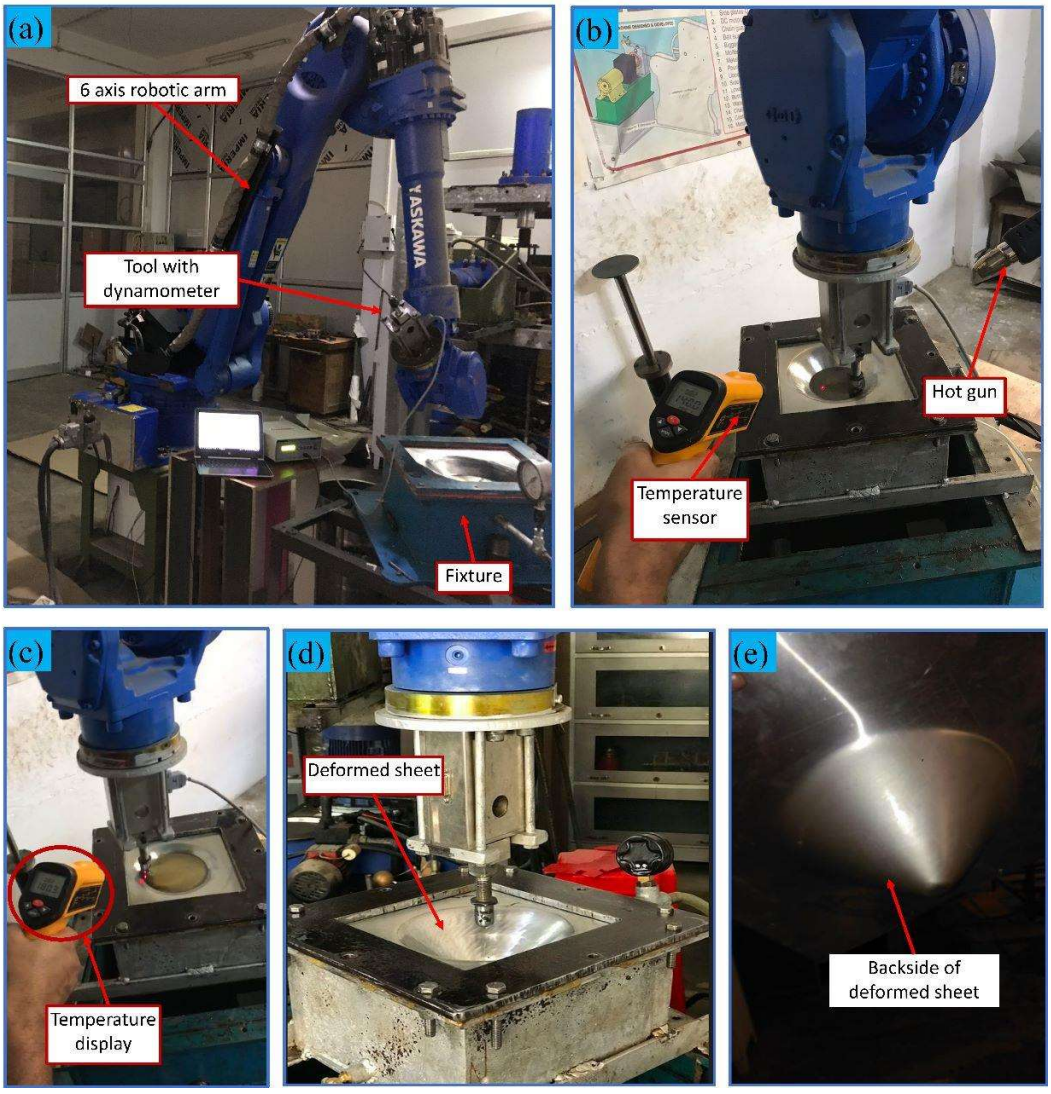

Figure 6.5: Robot-assisted incremental sheet hydroforming setup: (a) labeled diagram of existing setup, (b) setup with temperature measurement and hot gun, (c) temperature display device, (d) experimentally formed cone showing inner surface along with tool, and (e) experimentally formed cone showing outer surface of the cone.

For the comparison of formability, a fixed wall angle cone has been formed until the onset of fracture. The maximum wall angle achieved in the case of CISF was 68° in and 76° for WISF. The details of the geometry along with the experimental conditions are summarized in Table 6.4.

Table 6.4: Experimental details for CISF and WISF.

Experimental Parameters	CISF	WISF
Sheet thickness	1.05 mm	1.05 mm
Tool type	Non revolving	Non revolving
Tool diameter	12.5 mm	12.5 mm
Tool speed	100 mm/s	100 mm/s
Initial circle diameter	240 mm	240 mm
Step depth	0.5 mm	0.5 mm
Max Wall angle of cone	68°	76°
No of cycles Run	160	160
Expected depth of cone	80 mm	80 mm
Achieved depth of cone	72.2 mm	74.6 mm
%Spring back	9.75%	6.75%

It can be concluded that larger deformation is achieved by WISF than CISF; additionally, it has been also observed that spring back is reduced in the case of WISF. This may be because of the softening of the sheet at elevated temperature. A 45° wall angle cone has been chosen for comparison of both the processes. Cones have been successfully formed by both the processes, using the optimized input parameters by the straight groove test, and a tool dynamometer has been used to measure forming force during the forming operation.

6.5 Results and discussion

6.5.1 Forming force

For the validation of simulation, the forming forces appearing in both RACISF and RAWISF were measured using a drill tool dynamometer, and the setup is shown in Figure 5.5(a). The capacity of the dynamometer was 500 kgf and had a strain-gauge-based 350 Ω bridge sensor. The force was measured in X, Y, and Z directions, and the result of all the three components was calculated. The forces measured from experiments and evaluated from simulation analysis have been compared by plotting graphs of various force components vs. time.

6.5.1.1 Comparison of forces in X direction (F_x)

The force in the X direction was evaluated from ABAQUS analysis of CISF and WISF. The force component in X direction was measured for both processes experimentally for validation. It has been found that the average force in X direction, in the case of warm forming determined reduced by 37.05%. The average and peak values of Fx in various cases are given in Table 6.5.

Table 6.5: Average and peak values of F_x evaluated from FEA model and experimentally.

Model	Average Force in CISF (N)	Average Force in WISF (N)	Peak Force in CISF (N)	Peak Force in WISF (N)
FEA Model	850.32	513.25	1213.79	962.43
Experimental	791.27	498.10	1316.66	1049.62

The variation in F_x in CISF and WISF with time obtained from the FEA model and measured experimentally is shown in Figure 6.6(a) and 6.6(b) respectively.

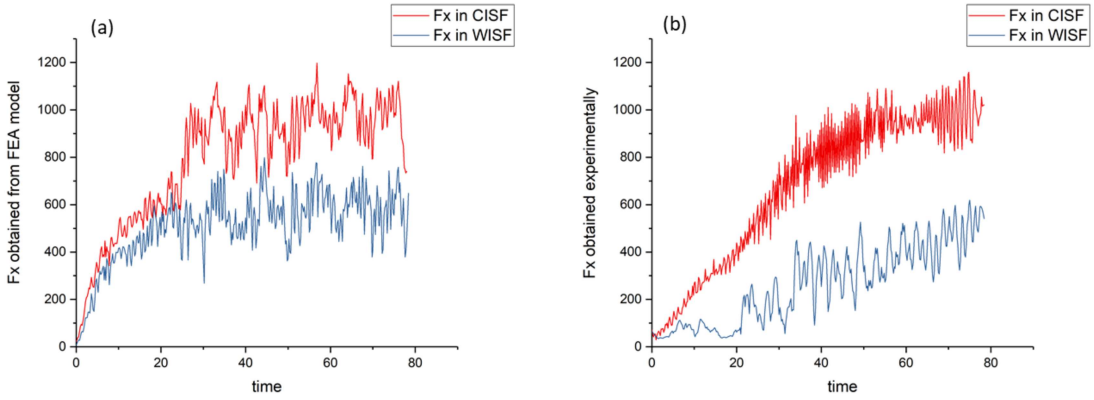

.

Figure 6.6: Comparison of X-component of forming force: (a) from FEA model and (b) measured experimentally.

6.5.1.2 Comparison of forces in Y direction (F_y)

The average force and peak force in the Y direction, obtained from the FEA model and measured experimentally, are given in Table 6.6.

Table 6.6. Average and peak values of F_Y obtained from FEA model and experimentally

Model	Average Force in CISF (N)	Average Force in WISF (N)	Peak Force in CISF (N)	Peak Force in WISF (N)
FEA Model	710.20	441.83	1402.79	838.48.43
Experimental	662.14	381.10	1038.66	930.62

As can be seen from Table 6.6, the average force in the Y direction determined experimentally has decreased by 42.45%, which closely matches with that predicted by FEA model. The variation of F_y obtained from FEA model and experiments for CISF and WISF with time is shown in Figure 6.7.

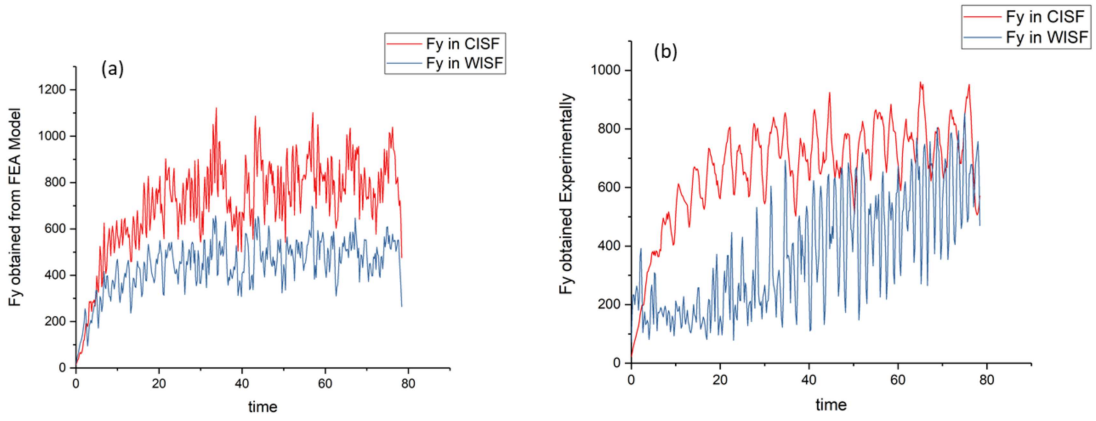

Figure 6.7: Comparison of Y-component of forming force: (a) FEA model and (b) measured experimentally.

6.5.1.3 Comparison of forces in Z direction (F_Z)

The values of average force and peak force in the Z direction by the FEA model and determined experimentally are presented in Table 6.7.

Table 6.7: Average and peak values of F_Z from the FEA model and experimentally.

Model	Average Force in CISF (N)	Average Force in WISF (N)	Peak Force in CISF (N)	Peak Force in WISF (N)
FEA Model	1371.82	690.45	2016.5	1007.31
Experimental	1362.65	635.92	1991.65	999.56

As seen from Tables 6.5–6.7, the Z-component of the forming force is the largest in magnitude. The Z-component of forming force evaluated experimentally in the case of warm forming is reduced by 53.32%. The variation in F_Z from the FEA model and experiments, with time, is shown in Figure 6.8.

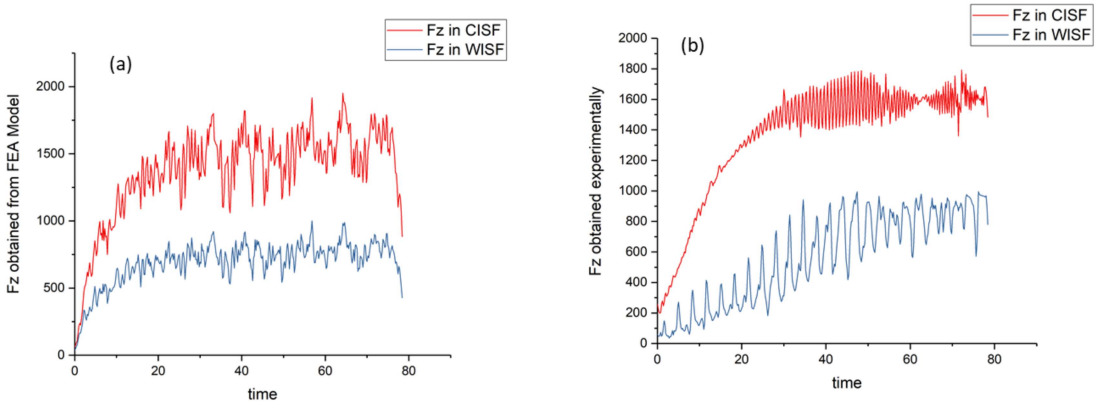

Figure 6.8: Comparison of Z-component of forming force: (a) FEA modelling and (b) obtained experimentally.

6.5.1.4 Comparison of total force in CISF and WISF (F_t)

The total forming force is found to decrease in the case of WISF. The loads on drives used in incremental sheet forming can be reduced significantly by using WISF. The average and peak values of the total forming force (Ft) in FEA and experimental analysis are presented in Table 6.8.

Table 6.8: Average and peak values of F_t obtained from FEA model and experimentally

Model	Average Force in CISF	Average Force in WISF	Peak Force in CISF	Peak Force in WISF
FEA Model	1741.16 N	969.17 N	2484.96 N	1444.73
Experimental	1672.84 N	739.75 N	2204.01 N	1388.69

As can be seen from Table 8, that the average force obtained from experiments is reduced by 55.77%. The variation total forming force for CISF and WISF from FEA model and evaluated experimentally, with time is shown in Figure 6.9.

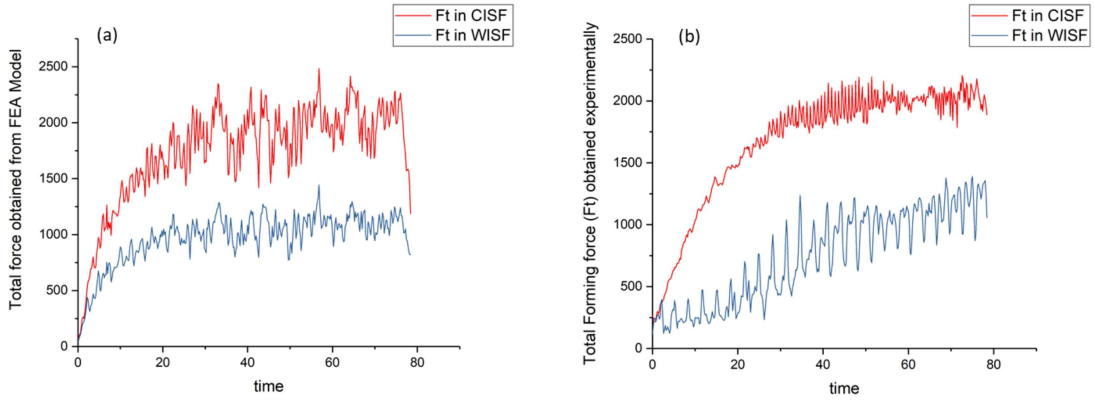

Figure 6.9: Comparison of total forming force: (a) FEA model and (b) determined experimentally.

It can be observed from Figure 6.9, that the forming force in the case of cold forming increases steeply in the beginning of the process and then increases at a slower rate and finally stabilizes. Almost the same trend has been found in the case of warm forming. The surface plot of all force components Fx, Fy, and Fz in CISF and WISF is shown in Figure 6.10. It can be seen from Figure 6.10 that all the components of forces increase during the fabrication of the cone in CISF and WISF. However, the force components in WISF were smaller than those in CISF.

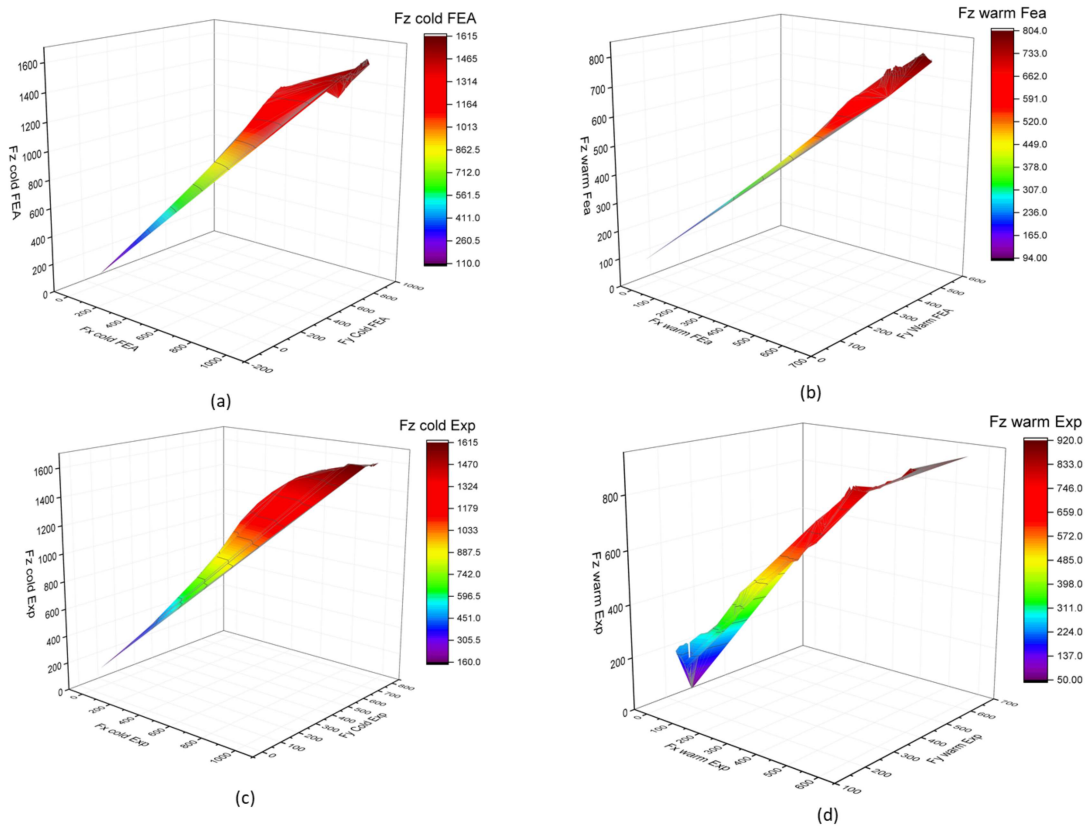

Figure 6.10: Three-dimensional surface plots of various force components during forming: (a) for CISF in FEA, (b) for WISF in FEA, (c) for experimental CISF, and (d) for experimental WISF.

6.5.2 Tensile test

Uniaxial tensile tests have been performed on a 100 kN INSTRON (MODEL 8801) universal tensile testing machine on samples made from undeformed sheets (Table 6.2) and the cones formed by the CISF and WISF. The samples were prepared as per the ASTM/E8 standard. The samples from the formed cones were cut in three different directions to examine the anisotropic effect on the formed component; namely, (a) along the length of the cone wall to evaluate tensile properties in the meridional directional; (b) along the circumferential direction of tool motion to evaluate the tensile properties in the transverse direction; (c) at 45° to the longitudinal direction along the surface of the cone. The tensile

samples cut from the formed cone is illustrated in Figure 6.11(b). Tensile testing was carried out at a crosshead speed of 1 mm/s. Figure 6.11(a) displays the specimens mounted on the uniaxial tensile testing and Figure 6.11(c) shows the specimen after breakage.

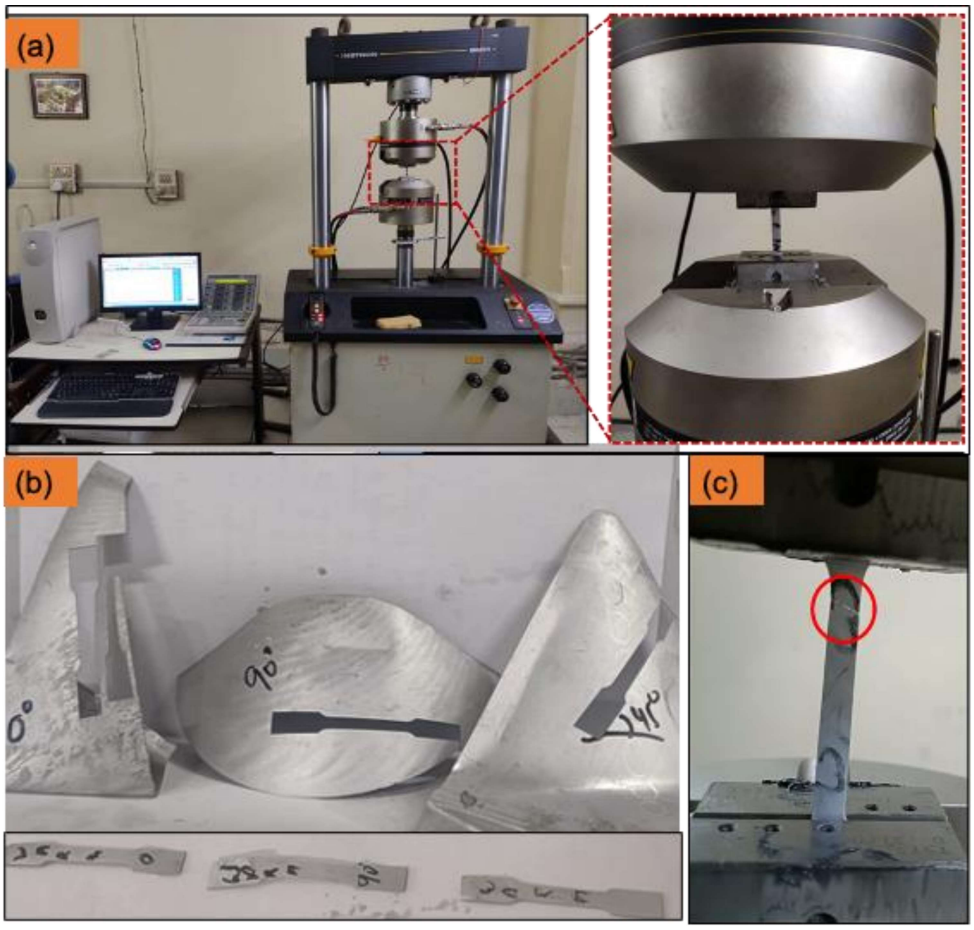

Figure 6.11: (a) UTM setup for tensile testing with mounted sample, (b) slots made after cutting of tensile samples in three directions: along the length of cone in the direction of tool (circumferential direction), and in the direction of 45° to the tool direction along the surface of the cone and respective samples after cutting, and (c) fracture region in red circle.

Engineering tensile stress–strain curves and true stress–true strain curves of samples are shown in Figure 6.12. The true stress is shown until UTS in all the cases.

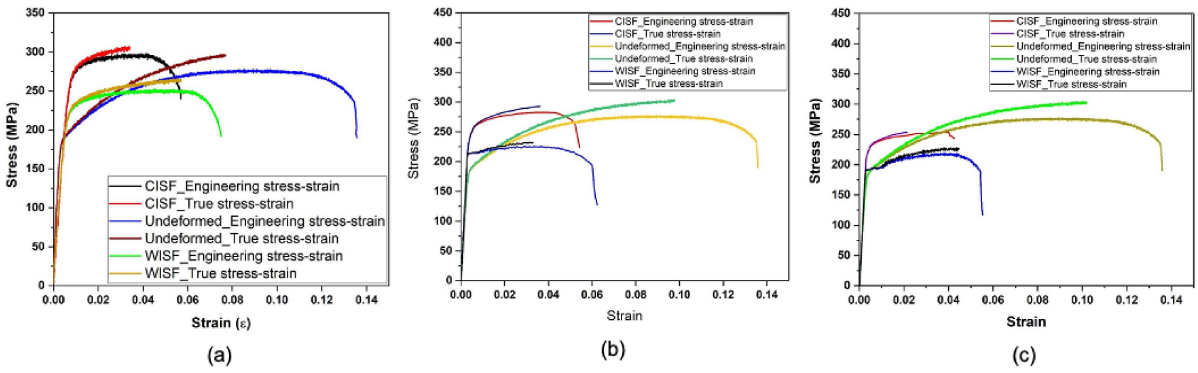

Figure 6.12: Comparison of tensile properties in the undeformed, CISF, and WISF conditions: (a) Along the length of cone, (b) Along the circumferential direction, and (c) In the 45° orientation.

The tensile properties evaluated from the tensile test in all three directions are given in Table 6.9. It can be observed from Table 6.9 that the tensile properties are affected by the orientation of test sample. Tensile strength as well ductility of the formed cones are different in different orientation; thus, there is an anisotropy in the formed cones and the effect of anisotropy on different parameters is different on the cones formed by CISF and WISF. However, properties obtained for the undeformed, CISF, and WISF samples showed some common trends. It has been found that, out of all three samples, the cone formed by CISF showed the maximum tensile strength. This is due to increased strain hardening induced in the sheet during cold forming. The strength of the cone formed by WISF exhibited higher ductility than the cone formed by CISF, which can be due to softening of the sheet at elevated temperature. It can be seen from the tensile test that there was a decrease in strength after warm working. Some controlled heat treatments can be given to fabricated parts to restore their strength.

Table 6.9: Effect of orientation on tensile properties of the cone formed by CISF and WISF.

Tensile properties along the length of the cone (meridional direction)			
Parameters	As received	CISF	WISF
0.2% offset Yield Strength (MPa)	249.30	192.31	183.26
UTS (MPa)	274. 54	289.06	244.39
Uniform elongation (%)	8.35	4.15	4.06
Elongation (%)	14.5	5.23	5.94
Tensile properties along circumference of cone			
0.2% offset Yield Strength (MPa)	249.30	213.65	201.98
UTS (MPa)	274. 54	279.51	216.65
Uniform elongation (%)	8.35	3.94	4.36
Elongation (%)	14.5	4.23	5.54
Tensile properties of the cone along 45 degrees			
0.2% offset yield strength (MPa)	249.30	206.12	197.36
UTS (MPa)	274. 54	281.83	224.26
Uniform elongation (%)	8.35	3.94	4.36
Elongation (%)	14.5	4.23	5.54

6.5.3 Microhardness test

It is crucial for sheet-metal-fabricated items to be strong and hard; therefore, the hardness of the sheet following CISF and WISF needs to be evaluated. Microhardness test has been conducted using the OMNITECH microhardness testing machine to compare the hardness of the sheet before and after forming the cone. The fabricated cone has been divided into 4 regions; 1, 2, 3, and 4. Region 1 is the upper undeformed region of the cone. Region 2, region 3, and region 4 are the cone's upper, middle, and lower regions, respectively, as shown in Figure 6.13(b). For each region, four microhardness measurements have been

taken at different points on the samples, and an average of the four values has been taken as the microhardness of that region. The respective microhardness values of the cones of the aluminum alloy 6061 formed by CISF and WISF are recorded in Table 6.10, and their graphical representation is displayed in Figure 6.13(a).

Table 6.10: Average microhardness of different regions of the formed cones.

Region	Microhardness ($HV_{0.2}$)		
	Undeformed	CISF	WISF
1	46.2	46	44.2
2	45.82	52.95	51.22
3	45.96	61.47	55.45
4	45.97	59.02	53.77

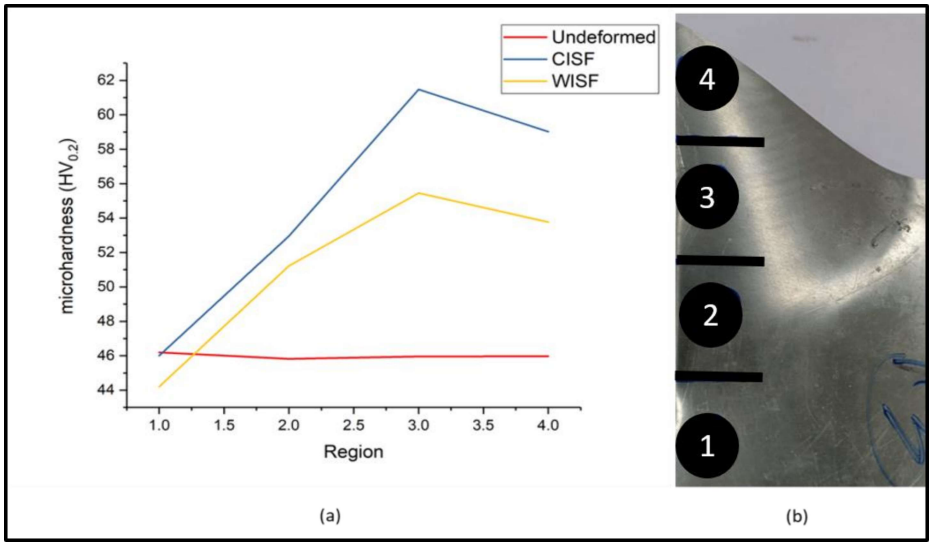

Figure 6.13: (a) Microhardness plots of the different regions of the undeformed sheet and (b) cones formed by CISF and WISF.

It can be seen that the microhardness in the CISF formed cone is maximum due to more effective strain hardening from cold working. Hardness is found to be highest in middle region of the cone, suggesting that this region had undergone maximum strain and strain hardening. Microhardness of the sample from the cone formed by WISF in different regions, is less than that of the sample from the cone formed by CISF. This test suggests that there can be a loss of hardness of the product formed by WISF, and suiTable heat treatment should be given to the fabricated part to increase the hardness.

6.5.4 Thickness distribution

A certain amount of sheet thinning is always associated with the ISF process. Thinning during the ISF process is attributed to thickness strain along the thickness direction. Sheet thickness in the formed cone can be roughly predicted by the famous sine law $t = t_0 \sin \theta$. Ambrogio et al. [138] showed that the thickness prediction by the sine law is most accurate in the middle region of the formed cone. To examine the sheet thickness along the wall of the formed cone, the formed region has been divided into 7 sub-regions (0–6), as shown in Figure 6.14 a, and the thickness in different regions has been measured by a micrometer with a pointed tip (Figure 6.14 b) and with a minor count of 0.001 mm. Region-0 is the undeformed region where the thickness was 1.05 mm, and region-6 is the lower undeformed region where the material accumulates as the tool drags the material with it; hence, the sheet thickness is found to be more in this region. However, in the regions 1–5 sheet thinning occurred. The average sheet thickness, t_{avg} (average of sheet thickness) in regions 1–5 in both the processes is given in Table 6.11. The thickness plots for CISF and WISF are shown in Figure 6.14(c). The yellow line shows the thickness predicted by the sine law for spinning ($t = t_0 \sin \theta$).

Table 6.11: Thickness distribution in the fabricated sheet of 6061 aluminum alloy in CISF and WISF

Process Used	Average Sheet Thickness in the Region 1–5 (t_{avg}) (mm)
CISF	0.809
WISF	0.783

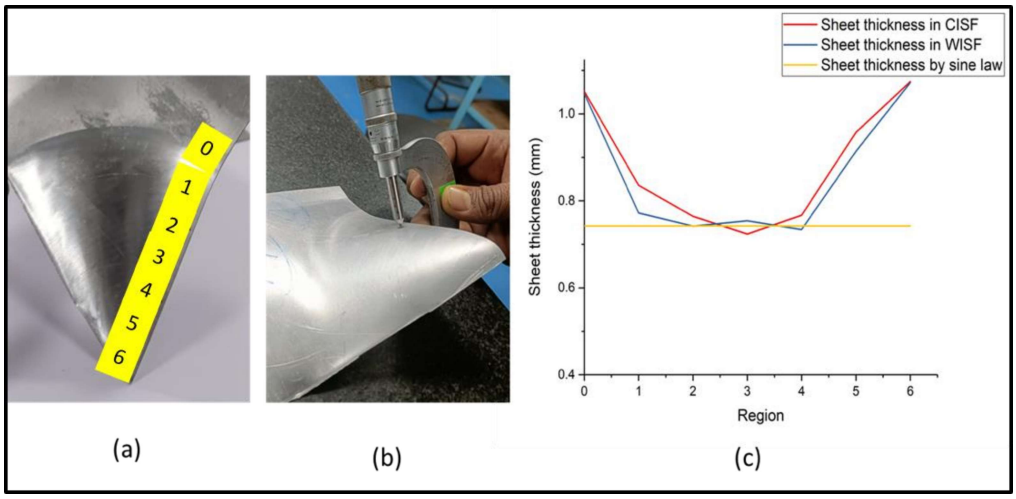

Figure 6.14: (a) Different regions for thickness measurement in formed cone, (b) measurement of sheet thickness by pointed-tip micrometer, and (c) thickness variation in different regions in CISF, WISF, and by sine law prediction.

It can be seen from Table 11 that the average sheet thickness in the case of CISF was more than that in WISF; however, the distribution of sheet thickness in the middle region of the cone was more uniform in the case of WISF. Hence, formability of the sheet by warm ISF is higher, and there can be a more uniform thickness distribution in the formed sheet.

6.5.5 Surface finish

The roughness of the cones produced by the CISF and WISF methods has been measured. Surface finish is an essential component of sheet metal forming operations; hence, the

impact of the forming process on the surface finish has been examined. To assess the surface quality before and after forming, the surface finish of the inner side and outer side of the cone has been measured and compared. As the inner side of the cone remains in direct contact of the forming tool, this side is likely to be rougher than that of the outer surface. For comparison, the sample was taken from the region 4, as this surface underwent maximum thinning. The test has been carried out on the Mitutoyo Surftest SV-2100 machine. The sampling length was 0.8 mm, the number of samplings was 5, and the travel length was 4.8 mm. The surface roughness of the undeformed and deformed sheet was examined by Ra, Rz, and Rq values. The corresponding values were measured by moving the stylus knob over the sample. The measured values are given in Table 6.12.

Table 6.12: Two-dimensional surface roughness of both surfaces of the cone, measured by surface roughness tester.

Component - Tool Contact Surface				Free Surface		
	R_a (µm)	R_z (µm)	R_q (µm)	R_a (µm)	R_z (µm)	R_q (µm)
Un-deformed	0.78	5.35	1.03	0.78	5.35	1.03
Cold formed	1.49	8.01	1.93	0.67	4.93	0.87
Warm formed	1.52	10.20	2.00	0.89	5.76	1.14

It can be seen from Table 12 that surface finish in the case of CISF was better than that in WISF. However, the variation was not much and can be accepted because of other benefits of WISF over CISF. To verify the same, the contact surface has been examined by an atomic force microscope. The AFM surface profile is shown in Figure 6.15.

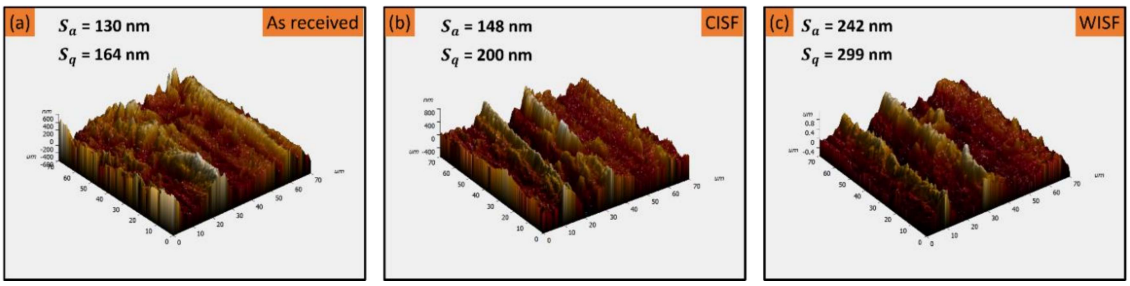

Figure 6.15: AFM surface profile of the sheet: (a) undeformed, (b) cone formed by CISF, and (c) cone formed by WISF.

It can also be seen from AFM analysis of the surface shown in Figure 15 that the surface obtained by WISF is of the most inferior quality. WISF affects the surface quality of the formed component; however, the surface is likely to be better than that achieved by hot forming, which can be the subject of further research.

6.6 Conclusions

In this Chapter, CISF and WISF were performed on aluminum alloy 6061, and the effect of warm forming on ISF was analyzed. FEA analysis was carried out for both the processes, and forming forces were calculated using FEA analysis on ABAQUS. Experiments were carried out to compare the two processes. Tensile and Erichsen ductility tests were performed to evaluate the tensile properties and formability of the sheets before deformation. Several shapes were made using the two processes, and their properties were compared. Experiments with parameters optimized by a straight groove test were performed, and the following conclusions are drawn.

- Warm forming significantly reduces the forming forces.
- Warm forming enhances the formability of the sheet, as evident from the larger wall angle of the cone formed by WISF.

- The strength of the product formed by CISF is higher than that formed by WISF; however, ductility increases in WISF, and hence more formability is achieved in WISF than in CISF.
- The uniformity of sheet thickness is found to be better in WISF than in CISF.
- The measurement of Ra, Rz, and Rq values revealed that WISF adversely affects the surface quality of the formed component; hence, some post-processing can be required.
- WISF can be beneficial as it does not require addition of any sophisticated mounting, and properties of the products are enhanced.